Impedance-Decoupled Modelling Method of Multi-Port Transmission Network in Inverter-Fed Power Plant

Zhou, Weihua; Wang, Yanbo; Chen, Zhe

Published in:
I E E E Transactions on Industry Applications

DOI (link to publication from Publisher):
10.1109/TIA.2019.2951387

Publication date:
2020

Document Version
Accepted author manuscript, peer reviewed version

Impedance-Decoupled Modelling Method of Multi-Port Transmission Network in Inverter-Fed Power Plant

Weihua Zhou, *Student Member, IEEE*, Yanbo Wang, *Senior Member, IEEE*, and Zhe Chen, *Fellow, IEEE*

***Abstract*—This paper presents an impedance-decoupled modelling method of multi-port transmission network in an inverter-fed power plant, which is able to simplify modelling and stability analysis procedure for power plant with complicated transmission network. Impedance-decoupled models of three-port and four-port transmission networks are first established. On the basis of them, impedance-decoupled model of multi-port transmission network is derived, where transmission node with multiple branches is modelled by means of Norton equivalent circuit. Furthermore, based on the proposed impedance-decoupled network modelling method, the whole power plant is divided into multiple subsystems, and Nyquist stability criterion is performed for all subsystems, where oscillation source can be identified in an explicit way. Simulation and experimental results are given to validate effectiveness of the proposed impedance-decoupled modelling and stability analysis method. The proposed modelling method is able to simplify modelling procedure of large-scale power plant with complicated transmission network, which is also applicable in power plant with various transmission network topologies.**

***Index Terms*—Impedance-based stability analysis, impedance-decoupled modelling, inverter-fed power plant, Nyquist stability criterion, oscillation source identification, transmission network.**

I. Introduction

THE increasing penetration of renewable energies such as wind energy and solar energy are promoting the application of distributed power generation. Solid state interface-based power converters are intensively adopted to integrate renewable energies into power systems [1]. To enhance power quality, passive components such as L and LCL filters are commonly used to mitigate high-order switching ripples. However, the interaction between inner control loops and passive components can cause system resonance as variation of grid impedance in a wide frequency range [2]–[6]. Therefore, it is significant to develop modelling and analysis method for revealing mechanism and identifying possibility of oscillation phenomena at early planning stage of inverter-fed power plant.

Impedance-based stability criterion (IBSC) has been originally proposed in [7] to assess stability issue of single grid-connected inverter (GCI)-based power plant. Furthermore, it was developed to assess stability issues of power system with multiple GCIs [8]–[21]. The method only needs terminal impedance frequency responses instead of detailed structure and parameters which are sometimes unknown due to industrial confidentiality [22]. However, it can only predict local stability issue at a specific point [7]. To identify global stability, IBSC should be performed at all buses, if right-half-plane (RHP) poles of impedance ratios of load and source parts are not calculated [9]–[11]. However, it is not easy to implement stability assessment in a large-scale power system with complicated transmission network. Existing works commonly simplify or ignore the characteristics of transmission lines (TLs) and power cables to perform stability assessment. For example, only TL impedance between point of common connection (PCC) and utility grid is considered in [12]–[18]. TLs impedance among GCIs are further considered in [10], [11]. In addition, TLs impedance among GCIs and buses are considered in [9], [20], [21]. However, these existing works slightly consider characteristics of complicated transmission network. A systematic impedance network modelling method is proposed in [23], [24] to quantitatively assess stability issue of large-scale wind power plants, where impedance matrices of all components are first established in a global dq frame. Then, system impedance matrix is calculated by aggregating individual impedance matrices using basic circuit principles. However, computation of system high-order impedance matrix tends to cause high computational burdens, which complicates stability analysis in large-scale inverter-fed power plants with complicated transmission network. A decoupled two-port impedance model of a long transmission cable is proposed in [20], [25] to simplify IBSC, where two terminals of the long transmission cable are represented as controlled voltage/current sources. However, the decoupled impedance modelling method fails to be applied in a multiple branch-based transmission network.

To perform stability analysis in the inverter-fed power plant with complicated transmission network, this paper presents an impedance-decoupled modelling method of multi-port transmission network. The overall system is first partitioned into multiple GCI units and TLs. Then, impedance models of all GCIs are represented in the form of Norton equivalent circuits, and TLs connected to the same node are modelled as a multi-port impedance model which is composed of several current/voltage controlled Norton equivalent circuits. Based on interconnection relationship among these GCI units and TLs, the impedance-decoupled network model of the power plant is formulated by combining these different components, and the

This work was supported by the ForskEL and EUDP project "Voltage Control and Protection for a Grid towards 100% Power Electronics and Cable Network (COPE)" (Project No.: 880063).

The authors are with the Department of Energy Technology, Aalborg University, Aalborg 9220, Denmark (e-mail: wez@et.aau.dk; ywa@et.aau.dk; zch@et.aau.dk).

whole power plant is divided into several subsystems. Stability analysis is then performed for all subsystems simultaneously, where the needed source and load impedance formulas are explicitly presented in the established impedance-decoupled network model. Therefore, the problematical GCIs can be identified once the Nyquist stability criterion is not satisfied, which cannot be achieved by either performing IBSC one time at a specific point or establishing the impedance network model, since dynamics of individual GCIs are lost during the impedance aggregation procedure [11], [23]. In addition, since the impedance models of GCIs and TLs are modelled independently, it's easy to re-calculate the impedance-decoupled network model providing that transmission network topology changes. Main advantages of the proposed impedance-decoupled network modelling method are explained as follows. (1) The modelling method is able to simplify stability analysis in the inverter-fed power plant with complicated transmission network. Also, the modelling method can be applied into various network structures. (2) The modular impedance network modelling method based on interconnection relationship of individual components is advantageous when transmission network topology changes. (3) The impedance-decoupled network model-based stability analysis procedure is able to identify oscillation sources.

The rest of the paper is organized as follows. In Section II, studied inverter-fed power plant is described, and drawbacks of existing IBSCs are explained. The principle of the proposed impedance-decoupled network modelling method is given in Section III. In Section IV, the implementation details of the proposed impedance-decoupled network modelling method for different network structures are given. Simulation and experimental results are provided in Section V to validate effectiveness of the proposed modelling method. Conclusions are drawn in Section VI.

II. System Description and Problem Formulation

Fig. 1 shows single line diagram of a grid-connected power plant, where inverter-fed power generators are integrated into utility grid by a radial transmission network [26]. According to the number of connected TLs, three kinds of nodes can be seen in Fig. 1, including three TLs-connected nodes $\times$, four TLs-connected nodes $*$ and five TLs-connected nodes $\otimes$.

Stability assessment can be performed by applying IBSC in different ways. The first one is to perform IBSC one time at a specific point with calculating RHP poles of impedance ratio of load and source parts. For example, if PCC in Fig. 1 is selected, according to the argument principle, the number of RHP zeros of $(1+\frac{Z_L}{Z_S})$ can be calculated as follows [7],

$$Z(1+\frac{Z_L}{Z_S}) = P(1+\frac{Z_L}{Z_S}) - N_{(-1,j0)}(\frac{Z_L}{Z_S}) \qquad (1)$$

where $Z(\bullet)$ and $P(\bullet)$ are the number of RHP zeros and RHP poles, respectively. $N_{(-1,j0)}(\bullet)$ is the encirclement number of Nyquist plot around $(-1, j0)$ in counterclockwise direction.

Based on (1), the encirclement number of the Nyquist plot of $\frac{Z_L}{Z_S}$ around $(-1, j0)$ and the number of RHP poles of $1+\frac{Z_L}{Z_S}$ should be calculated. However, impedance model with

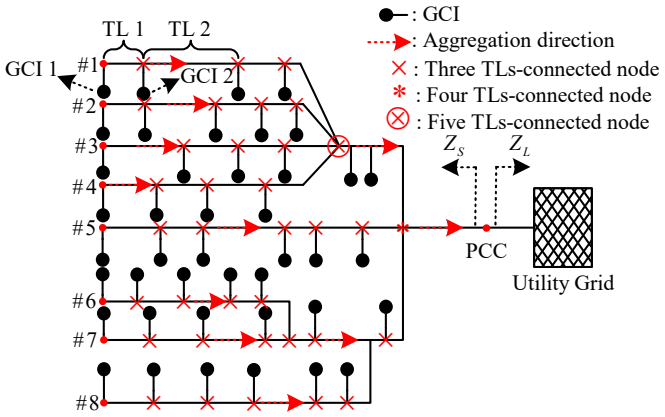

Fig. 1. Single line diagram of a grid-connected power plant.

multiple GCIs and TLs in system level is complicated, which tends to result in high computational burdens. In addition, the method can only obtain local stability analysis result at the PCC point, which cannot identify problematical components.

The second stability analysis procedure is to add system components such as GCI and TL step by step, where stability analysis is implemented at all buses without calculating RHP poles of the impedance ratios of load and source parts [9], [10]. For example, stability analysis is first performed between GCI 1 and TL 1 at system terminal bus #1. If the stability analysis result is that the subsystem is stable, GCI 1, TL 1 and GCI 2 are aggregated, also stability analysis is performed between the aggregated subsystem and TL 2. IBSC is performed repeatedly along the aggregation direction shown as the red dashed line in Fig. 1 until the Nyquist stability criterion is not satisfied or all components are aggregated. Similarly, stability analysis is also performed sequentially for other branches #2, #3..., #8.

The drawbacks of existing modelling and stability analysis procedure are summarized as following. (1) Oscillation sources cannot be identified, if Nyquist stability criterion is only performed one time at a specific point. (2) If Nyquist stability criterion is performed multiple times at different points, multiple impedance expressions should be calculated, which is tedious and time-consuming if a great number of GCIs are connected into the power plant. (3) Impedance expressions should be calculated again, if transmission network topology changes. Therefore, this paper proposes an impedance-decoupled network modelling method of complicated network to overcome these drawbacks.

III. Proposed Impedance-Decoupled Modelling Method of Transmission Network

In principle, GCIs can be modelled as Norton equivalent circuits [7]. One assumption is that if the TLs in Fig. 1 can also be represented as Norton equivalent circuits, the stability analysis procedure may be simplified. In this section, an impedance-decoupled modelling method of transmission network is proposed. On the basis of it, the impedance modelling method of inverter-fed power plant is developed, and corresponding modified IBSC is given.

A. Impedance-Decoupled Modelling of Transmission Network

The impedance-decoupled three-port and four-port models of three TLs-based and four TLs-based transmission networks are first established, followed by extension to multiple TLs-based transmission network.

1) Impedance-Decoupled Three-Port Model of Three TLs-Based Transmission Network: Fig. 2 shows a three TLs-based transmission network, where Z_1, Z_2, Z_3 are impedances of the three TLs (TL 4 is not considered here). v_1, v_2 and v_3 are three terminal voltages, respectively. The relationship of currents at node A is given by Kirchhoff's current law (KCL) as (2).

$$i_1 + i_2 + i_3 = \frac{v - v_1}{Z_1} + \frac{v - v_2}{Z_2} + \frac{v - v_3}{Z_3} = 0 \tag{2}$$

And voltage v of node A is given as (3).

$$v = f(v_1, v_2, v_3) = \frac{Z_1Z_2v_3 + Z_2Z_3v_1 + Z_1Z_3v_2}{Z_1Z_2 + Z_2Z_3 + Z_1Z_3} \tag{3}$$

Then, three branch currents i_1, i_2 and i_3 can be obtained by Ohm's law as (4).

$$\begin{aligned} i_1 &= \frac{v - v_1}{Z_1} = \frac{Z_2v_3 + Z_3v_2 - (Z_2 + Z_3)v_1}{Z_1Z_2 + Z_2Z_3 + Z_1Z_3} \\ i_2 &= \frac{v - v_2}{Z_2} = \frac{Z_1v_3 + Z_3v_1 - (Z_1 + Z_3)v_2}{Z_1Z_2 + Z_2Z_3 + Z_1Z_3} \\ i_3 &= \frac{v - v_3}{Z_3} = \frac{Z_1v_2 + Z_2v_1 - (Z_1 + Z_2)v_3}{Z_1Z_2 + Z_2Z_3 + Z_1Z_3} \end{aligned} \tag{4}$$

The branch currents equations in (4) can be rewritten as (5).

$$\begin{aligned} i_1 &= f_1(v_1, v_2, v_3) = -\frac{v_1}{Z_{1sh}} + i_1'(v_2, v_3) \\ i_2 &= f_2(v_1, v_2, v_3) = -\frac{v_2}{Z_{2sh}} + i_2'(v_1, v_3) \\ i_3 &= f_3(v_1, v_2, v_3) = -\frac{v_3}{Z_{3sh}} + i_3'(v_1, v_2) \end{aligned} \tag{5}$$

where

$$\begin{aligned} Z_{1sh} &= \frac{Z_1Z_2 + Z_2Z_3 + Z_1Z_3}{Z_2 + Z_3} \\ Z_{2sh} &= \frac{Z_1Z_2 + Z_2Z_3 + Z_1Z_3}{Z_1 + Z_3} \\ Z_{3sh} &= \frac{Z_1Z_2 + Z_2Z_3 + Z_1Z_3}{Z_1 + Z_2} \end{aligned} \tag{6}$$

$$\begin{aligned} i_1'(v_2, v_3) &= \frac{Z_2v_3 + Z_3v_2}{Z_1Z_2 + Z_2Z_3 + Z_1Z_3} \\ i_2'(v_1, v_3) &= \frac{Z_1v_3 + Z_3v_1}{Z_1Z_2 + Z_2Z_3 + Z_1Z_3} \\ i_3'(v_1, v_2) &= \frac{Z_1v_2 + Z_2v_1}{Z_1Z_2 + Z_2Z_3 + Z_1Z_3} \end{aligned} \tag{7}$$

The impedance-decoupled three-port model can be established as shown in Fig. 3 according to (5). The three impedances of the Norton equivalent circuits Z_{1sh}, Z_{2sh} and Z_{3sh} in Fig. 3 are actually the three terminal impedances with the other two terminals short-circuited Z_{short1}, Z_{short2} and Z_{short3}, derived as (8).

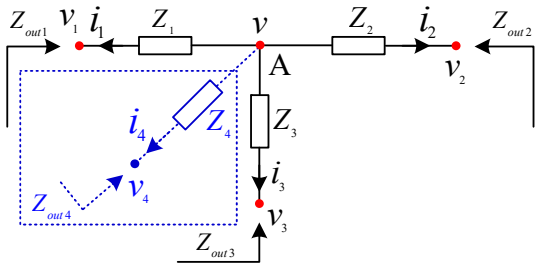

Fig. 2. Three/Four TLs-based transmission network.

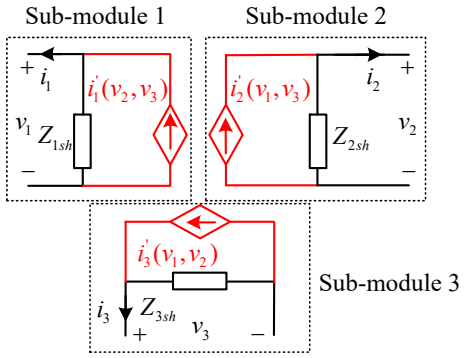

Fig. 3. Impedance-decoupled three-port model of three TLs-based transmission network as shown in Fig. 2.

$$\begin{aligned} Z_{1sh} &= \left.\frac{-v_1}{\frac{-v_1}{Z_{1sh}} + i_1'}\right|_{i_1'=0} = \left.\frac{-v_1}{i_1}\right|_{v_2=v_3=0} = Z_{short1} \\ Z_{2sh} &= \left.\frac{-v_2}{\frac{-v_2}{Z_{2sh}} + i_2'}\right|_{i_2'=0} = \left.\frac{-v_2}{i_2}\right|_{v_1=v_3=0} = Z_{short2} \\ Z_{3sh} &= \left.\frac{-v_3}{\frac{-v_3}{Z_{3sh}} + i_3'}\right|_{i_3'=0} = \left.\frac{-v_3}{i_3}\right|_{v_1=v_2=0} = Z_{short3} \end{aligned} \tag{8}$$

It can be seen that the impedance-decoupled three-port model of the three TLs-based transmission network makes the terminal impedance with the other two terminals short-circuited apparent and visible. In addition, three voltage-controlled current sources $i_1'(v_2, v_3)$, $i_2'(v_1, v_3)$ and $i_3'(v_1, v_2)$ shown as the red lines in Fig. 3 can be neglected in the further IBSC.

Note that the established equivalent circuit model of the three-port transmission network itself is actually not decoupled, since $i_1'(v_2, v_3)$, $i_2'(v_1, v_3)$ and $i_3'(v_1, v_2)$ are determined by two terminal voltages at the other two ends, as shown in (7). $i_1'(v_2, v_3)$, $i_2'(v_1, v_3)$ and $i_3'(v_1, v_2)$ are neglected in the further IBSC, and Z_{1sh}, Z_{2sh} and Z_{3sh} are not influenced by the other two sub-modules. Therefore, the term "impedance-decoupled three-port model" is used here to show that the three impedances are decoupled when compared with Fig. 2 where three impedances Z_1, Z_2 and Z_3 are coupled via node A.

2) Impedance-Decoupled Four-Port Model of Four TLs-Based Transmission Network: Based on the derivation process of impedance-decoupled three-port model of three TLs-based transmission network, an impedance-decoupled four-

port model of the transmission network in Fig. 2 can be established (TL 4 is considered here), as shown in Fig. 4. The detailed representations of impedances and voltage-controlled current sources are shown as (9) and (10), respectively.

$$\begin{aligned} Z^*_{1sh} &= \frac{Z_2Z_3Z_4 + Z_1Z_3Z_4 + Z_1Z_2Z_4 + Z_1Z_2Z_3}{Z_3Z_4 + Z_2Z_4 + Z_2Z_3} \\ Z^*_{2sh} &= \frac{Z_2Z_3Z_4 + Z_1Z_3Z_4 + Z_1Z_2Z_4 + Z_1Z_2Z_3}{Z_3Z_4 + Z_1Z_4 + Z_1Z_3} \\ Z^*_{3sh} &= \frac{Z_2Z_3Z_4 + Z_1Z_3Z_4 + Z_1Z_2Z_4 + Z_1Z_2Z_3}{Z_2Z_4 + Z_1Z_4 + Z_1Z_2} \\ Z^*_{4sh} &= \frac{Z_2Z_3Z_4 + Z_1Z_3Z_4 + Z_1Z_2Z_4 + Z_1Z_2Z_3}{Z_2Z_3 + Z_1Z_3 + Z_1Z_2} \end{aligned} \tag{9}$$

$$\begin{aligned} i^*_1(v_2,v_3,v_4) &= \frac{Z_3Z_4v_2 + Z_2Z_4v_3 + Z_2Z_3v_4}{Z_2Z_3Z_4 + Z_1Z_3Z_4 + Z_1Z_2Z_4 + Z_1Z_2Z_3} \\ i^*_2(v_1,v_3,v_4) &= \frac{Z_1Z_4v_3 + Z_1Z_3v_4 + Z_3Z_4v_1}{Z_2Z_3Z_4 + Z_1Z_3Z_4 + Z_1Z_2Z_4 + Z_1Z_2Z_3} \\ i^*_3(v_1,v_2,v_4) &= \frac{Z_1Z_2v_4 + Z_2Z_4v_1 + Z_1Z_4v_2}{Z_2Z_3Z_4 + Z_1Z_3Z_4 + Z_1Z_2Z_4 + Z_1Z_2Z_3} \\ i^*_4(v_1,v_2,v_3) &= \frac{Z_1Z_2v_3 + Z_2Z_3v_1 + Z_3Z_1v_2}{Z_2Z_3Z_4 + Z_1Z_3Z_4 + Z_1Z_2Z_4 + Z_1Z_2Z_3} \end{aligned} \tag{10}$$

Similar with Z_{1sh}, Z_{2sh} and Z_{3sh} in Fig. 3, Z^*_{1sh}, Z^*_{2sh}, Z^*_{3sh} and Z^*_{4sh} are the four terminal impedances with the other three terminals short-circuited. Four voltage-controlled current sources $i^*_1(v_2,v_3,v_4)$, $i^*_2(v_1,v_3,v_4)$, $i^*_3(v_1,v_2,v_4)$ and $i^*_4(v_1,v_2,v_3)$ shown as the red lines in Fig. 4 can be omitted in the further IBSC.

3) Impedance-Decoupled Multi-Port Model of Multiple TLs-Based Transmission Network: In order not to lose generality, the impedance representations of the impedance-decoupled m-port model of the m TLs-based transmission network are derived and shown as (11).

$$Z_{ksh} = \frac{\sum_{i=1}^{m}\left(\prod_{j=1,j\neq i}^{m} Z_j\right)}{\sum_{i=1,i\neq k}^{m}\left(\prod_{j=1,j\neq i,j\neq k}^{m} Z_j\right)} \quad k = 1,2...m \tag{11}$$

Similar with three/four TLs-based transmission network, Z_{ksh} is the kth terminal impedance with the other $m-1$ terminals short-circuited.

B. Implementation Procedure of the Proposed Impedance-Decoupled Network Modelling Method

The two steps-based implementation procedure of the proposed impedance-decoupled network modelling method for stability analysis of power plant is shown in Fig. 5.

- **Step 1: Establish the impedance-decoupled network model of power plant.** The overall system is first partitioned into individual GCI units and transmission networks. Norton equivalent circuits of GCI units are established, and corresponding terminal impedance formulas are calculated [8], [18]. Norton equivalent circuits of transmission networks can be established as Figs. 3 and 4. In addition, multiple TLs-based transmission network can be established as similar circuits. The circuit parameters are calculated by (8), (9) and (11). These Norton equivalent circuits of GCIs and transmission networks are then combined together based on their interconnection relationship.
- **Step 2: Perform IBSC to assess system stability issue.** An aggregation path is first identified. In principle, the aggregation direction should be from the farest bus to PCC, so that all components can be aggregated. Then, all components which are not on the aggregation path are aggregated. Finally, IBSC is performed for all the subsystems on the aggregation path simultaneously. If Nyquist stability criterion is satisfied for all the subsystems, the whole power plant is globally stable. Otherwise, if Nyquist stability criterion is not satisfied for any subsystems, the power plant is unstable, and problematical components are identified.

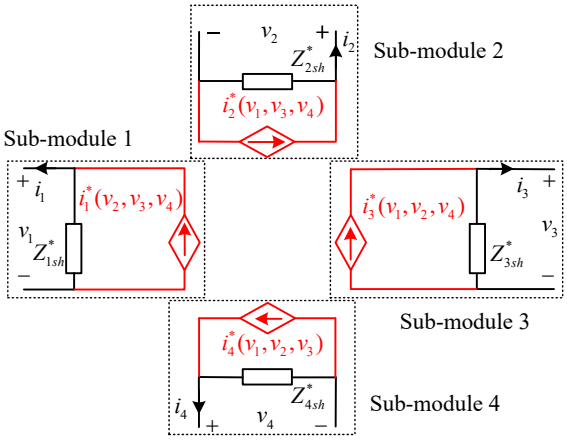

Fig. 4. Impedance-decoupled four-port model of four TLs-based transmission network as shown in Fig. 2.

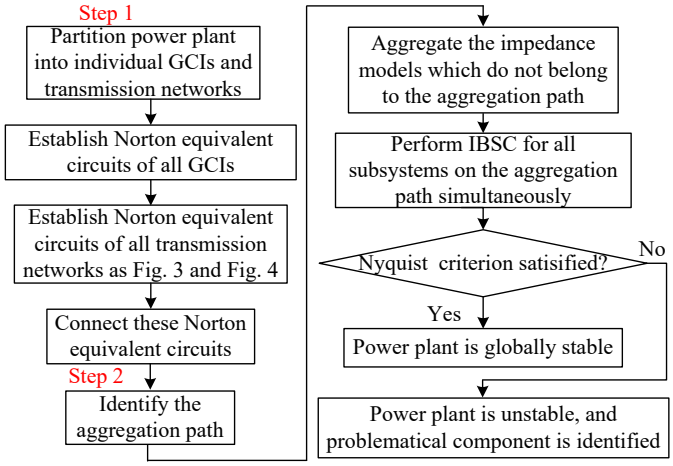

Fig. 5. Implementation procedure of stability analysis of power plant based on the proposed impedance-decoupled network modelling method.

To further validate the effectiveness of the proposed impedance-decoupled network modelling method, the detailed mathematical derivation is given here. Fig. 6(a) shows system equivalent circuit model of an M-GCIs-based radial power plant. i_g can be derived according to the superposition prin-

ciple of linear circuit. For example, effect of #1Inverter on i_g can be derived by ignoring the other $M-1$ current sources, shown as follows,

$$i_{g\_1} = G_{ii1} I^*_{ref1} \prod_{k=1}^{M} (1 + Z_k Z^{-1}_{Bk\_L})^{-1} \tag{12}$$

where Z_k is the TL impedance between bus k and bus $k+1$, Z_{Bk_L} is the total impedance of left part of bus k ($k = 1, 2..., M$). Z_{Bk_L} can be derived by recursive method, shown as follows,

$$\begin{aligned} &Z_{B1\_L} = Z_{inv1} \\ &Z_{B2\_L} = ((Z_{B1\_L} + Z_1)^{-1} + (Z_{inv2} + Z_{2T})^{-1})^{-1} \\ &Z_{B3\_L} = ((Z_{B2\_L} + Z_2)^{-1} + (Z_{inv3} + Z_{3T})^{-1})^{-1} \\ &\quad .... \\ &Z_{BM\_L} = ((Z_{B(M-1)\_L} + Z_{M-1})^{-1} + (Z_{invM} + Z_{MT})^{-1})^{-1} \end{aligned} \tag{13}$$

Similarly, i_{g_j} ($j = 2, 3..., M$) can be derived as follows,

$$i_{g\_j} = G_{iij} I^*_{refj} \prod_{k=j}^{M} (1 + Z_k Z^{-1}_{Bk\_L})^{-1} \tag{14}$$

Based on (12) and (14), the current source of the Norton equivalent circuit of left part of PCC can be calculated as follows,

$$I^*_{reftot} = \sum_{j=1}^{M} i_{g\_j} = \sum_{j=1}^{M} (G_{iij} I^*_{refj} \prod_{k=1}^{M} (1 + Z_k Z^{-1}_{Bk\_L})^{-1}) \tag{15}$$

In addition, the impedance of the Norton equivalent circuit of left part of PCC can be calculated as follows,

$$Z_{invtot} = Z_{BM\_L} + Z_M \tag{16}$$

The equivalent circuit model of Fig. 6(a) is shown in Fig. 6(b). i_g can then be expressed as follows,

$$i_g = (I^*_{reftot} - Z^{-1}_{invtot} V_g)(1 + Z_g Z^{-1}_{invtot})^{-1} \tag{17}$$

It can be seen from (15) and (17) that if $(1 + Z_k Z^{-1}_{Bk\_L})$ ($k = 1, 2..., M$) and $(1 + Z_g Z^{-1}_{invtot})$ do not have RHP zeros, i_g is stable. Based on the Cauchy's argument principle, the condition can be satisfied, if the Nyquist diagrams of $T_{m\_Bk\_1} = Z_k Z^{-1}_{Bk\_L}$ ($k = 1, 2..., M$) and $Z_g Z^{-1}_{invtot}$ do not encircle (-1, j0) in the complex plane [7]. $T_{m\_Bk\_1}$ is rewritten as follows,

$$T_{m\_Bk\_1} = \frac{Z_k}{Z_{Bk\_L}} = \frac{Z_{k\_1} + Z_{k\_2}}{Z_{Bk\_L}} = \frac{N_1}{D_1} \tag{18}$$

In the proposed impedance-decoupled network modelling method, Z_k is divided into two parts Z_{k_1} and Z_{k_2}, and $Z_{1\_1} = Z_{2\_1} = ...Z_{M\_1}$. Whether the Nyquist plot of $T_{m\_Bk\_2}$ encircles $(-1, j0)$ is checked, shown as follows,

$$T_{m\_Bk\_2} = \frac{Z_{Bk\_sh}}{Z_{Bk\_L}(1 + \frac{Z_{k\_1}}{Z_{Bk\_L}})} = \frac{N_2}{D_2} \tag{19}$$

where Z_{Bk_sh} is the impedance of transmission network which consists of Z_{k_2}, $Z_{(k+1)\_1}$ and $Z_{(k+1)T}$, which can be calculated based on (6), shown as follows,

$$\begin{aligned} Z_{Bk\_sh} &= Z_{k\_2} + Z_{(k+1)\_1} // Z_{(k+1)T} \\ &= Z_{k\_2} + Z_{(k+1)\_1}(1 + \frac{Z_{(k+1)\_1}}{Z_{(k+1)T}})^{-1} \end{aligned} \tag{20}$$

By comparing (18) and (19), the following constraints can be obtained.

$$\begin{aligned} |Mag(N_2)| &< |Mag(N_1)| \\ |Mag(D_2)| &> |Mag(D_1)| \end{aligned} \tag{21}$$

Therefore,

$$|T_{m\_Bk\_1}| > |T_{m\_Bk\_2}| \tag{22}$$

It can be seen from (22) that, if Nyquist diagram of $T_{m\_Bk\_2}$ encircles $(-1, j0)$, i.e., $|T_{m\_Bk\_2}| > 1$, we have $|T_{m\_Bk\_1}| > 1$, i.e., the Nyquist diagram of $T_{m\_Bk\_1}$ also encircles $(-1, j0)$. Thus, the system is identified as unstable, and the instability phenomena result from the impedance interaction between bus k and bus $k+1$.

The aforementioned mathematical derivation procedure shows that the stability issue of the power plant can be assessed by the proposed impedance-decoupled network model. In addition, the subsystems which contribute to the instability phenomena can be identified, once Nyquist stability criterion is not satisfied.

IV. Stability Analysis Based on the Proposed Impedance-Decoupled Network Model

In this section, stability analysis is performed on the basis of the proposed impedance-decoupled network modelling method. Case 1 is an artificial three GCIs-based radial power plant, and case 2 is a modified CIGRE low voltage distribution system.

A. Case 1: Three GCIs-Based Radial Power Plant

Fig. 7(a) shows one-line diagram of the studied power plant consisting of three GCIs. Parameters of the three GCIs are assumed as the same, and shown in the second column of Table I. According to step 1 in Fig. 5. The impedance-decoupled network model of the studied power plant in Fig. 7(a) can be established, as shown in Fig. 7(b). The impedance formulas of the two impedance-decoupled three-port network models are shown as (23).

$$\begin{aligned} Z_{11sh} &= \frac{Z_{TL1}Z_{TL2} + Z_{TL1}Z_{TL5} + Z_{TL2}Z_{TL5}}{Z_{TL2} + Z_{TL5}} \\ Z_{12sh} &= \frac{Z_{TL1}Z_{TL2} + Z_{TL1}Z_{TL5} + Z_{TL2}Z_{TL5}}{Z_{TL1} + Z_{TL5}} \\ Z_{13sh} &= \frac{Z_{TL1}Z_{TL2} + Z_{TL1}Z_{TL5} + Z_{TL2}Z_{TL5}}{Z_{TL1} + Z_{TL2}} \\ Z_{21sh} &= \frac{Z_{TL3}Z_{TL4} + Z_{TL4}Z_{TL6} + Z_{TL3}Z_{TL6}}{Z_{TL4} + Z_{TL6}} \\ Z_{22sh} &= \frac{Z_{TL3}Z_{TL4} + Z_{TL4}Z_{TL6} + Z_{TL3}Z_{TL6}}{Z_{TL3} + Z_{TL6}} \\ Z_{23sh} &= \frac{Z_{TL3}Z_{TL4} + Z_{TL4}Z_{TL6} + Z_{TL3}Z_{TL6}}{Z_{TL3} + Z_{TL4}} \end{aligned} \tag{23}$$

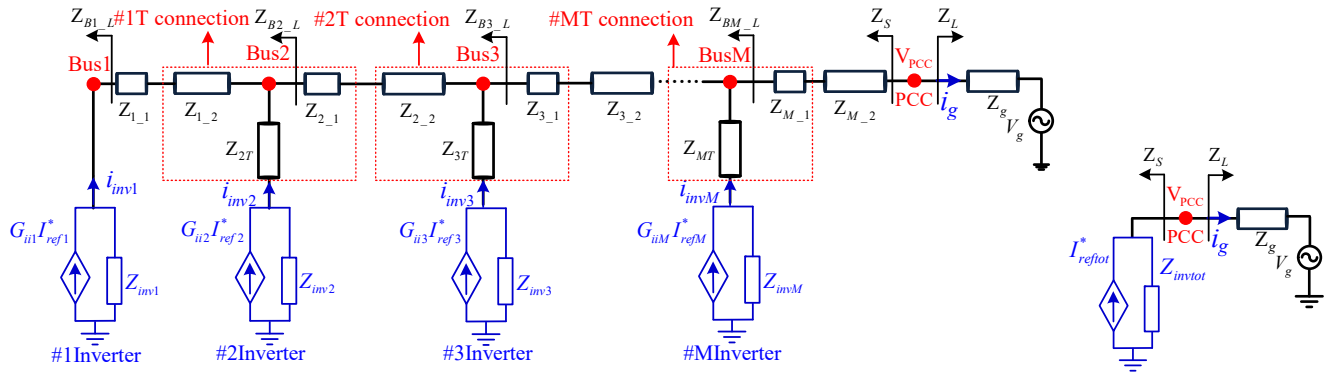

(a) (b)

Fig. 6. Illustration of the principle of the proposed impedance-decoupled network modelling method. (a) System impedance model of a radial power plant; (b) IBSC at PCC.

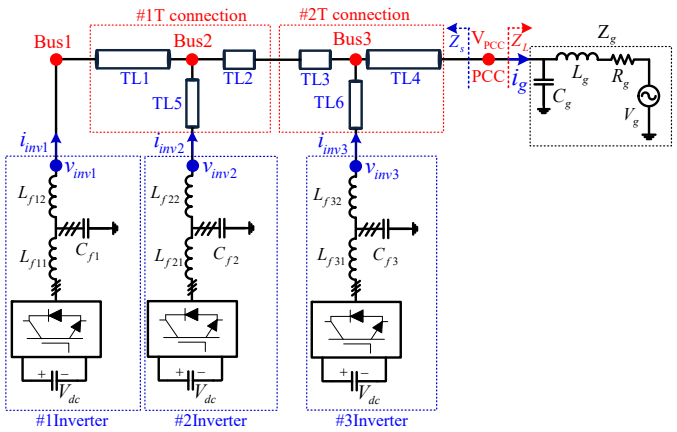

(a)

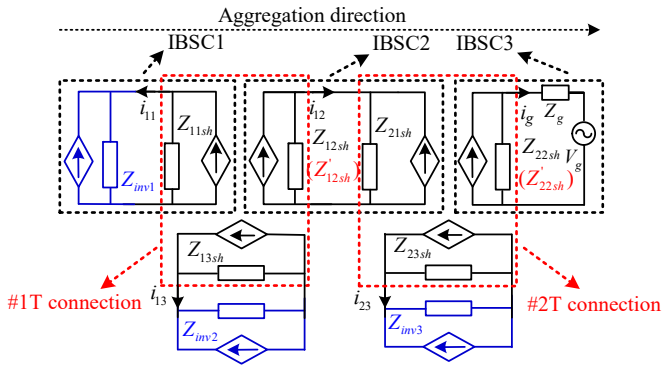

(b)

Fig. 7. Case 1. (a) One-line diagram of a three GCIs-based radial power plant; (b) Impedance-decoupled network model.

According to step 2 in Fig. 5, the aggregation path is identified in Fig. 7(b). Then, Z_{12sh} and Z_{22sh} are modified to include the terminal impedances of #1Inverter, #2Inverter and #3Inverter, shown as (24).

$$Z'_{12sh} = \frac{Z'_{TL1}Z_{TL2} + Z'_{TL1}Z'_{TL5} + Z_{TL2}Z'_{TL5}}{Z'_{TL1} + Z'_{TL5}}$$
$$Z'_{22sh} = \frac{Z'_{TL3}Z_{TL4} + Z_{TL4}Z'_{TL6} + Z'_{TL3}Z'_{TL6}}{Z'_{TL3} + Z'_{TL6}} \quad (24)$$

where $Z'_{TL1} = Z_{TL1} + Z_{inv1}$, $Z'_{TL5} = Z_{TL5} + Z_{inv2}$, $Z'_{TL3} = Z_{TL3} + Z'_{12sh}$ and $Z'_{TL6} = Z_{TL6} + Z_{inv3}$.

Then, Z_{11sh}/Z_{inv1}, Z_{21sh}/Z'_{12sh} and Z_g/Z'_{22sh} can be calculated to assess system stability issue. It can be seen that stability analysis of the original power system in Fig. 7(a) is achieved by assessing the stability of the three small decoupled subsystems in black dotted boxes in Fig. 7(b), which is easy to be extended if more GCIs are integrated into the power plant.

TABLE I
PARAMETERS OF THE GCIS AND GRID

Parameters	Case 1	Case 2
DC-link voltage V_{dc}	750V	750V
Grid fundamental frequency	50Hz	50Hz
Inverter side filter inductor L_{f1}	2mH	3mH
Grid side filter inductor L_{f2}	2mH	3mH
Filter capacitor C_f	6μF	5μF
Grid capacitance C_g	14μF	
Grid inductance L_g	1mH	
Grid resistance R_g	0.1Ω	
Switching frequency f_s	10kHz	10kHz
Sampling frequency f_{samp}	10kHz	10kHz
Grid voltage (phase-to-phase) V_g	380V	380V
Proportional gain of current controller K_p	7	9
Integral gain of current controller K_i	2000	2000
Proportional gain of PLL K_p	0.7	0.7
Integral gain of PLL K_i	3.2	3.2
Current reference value i_d^*	4A	30A
Current reference value i_q^*	0	0

To verify the effectiveness of the established impedance-decoupled network model in Fig. 7(b), two scenarios are investigated.

1) Scenario 1: If $L_{TL1} = L_{TL5} = L_{TL6} = 5$mH, $L_{TL2} = L_{TL3} = L_{TL4} = 0.5$mH, $C_g = 14\mu$F, $L_g = 1$mH and $R_g = 0.1\Omega$, Nyquist plots of three impedance ratios Z_{11sh}/Z_{inv1}, Z_{21sh}/Z'_{12sh} and Z_g/Z'_{22sh} are drawn in Fig. 8(a). It can be seen that IBSC1 and IBSC3 encircle point (-1, j0) one time, respectively, which indicates that the system is unstable. It can be concluded that the impedance interactions between left part and right part of bus 1 and PCC in Fig. 7(a) result in the instability phenomenon.

2) Scenario 2: The parameters in scenario 2 are the same as those in scenario 1, except that L_{TL1} is 1mH. The three

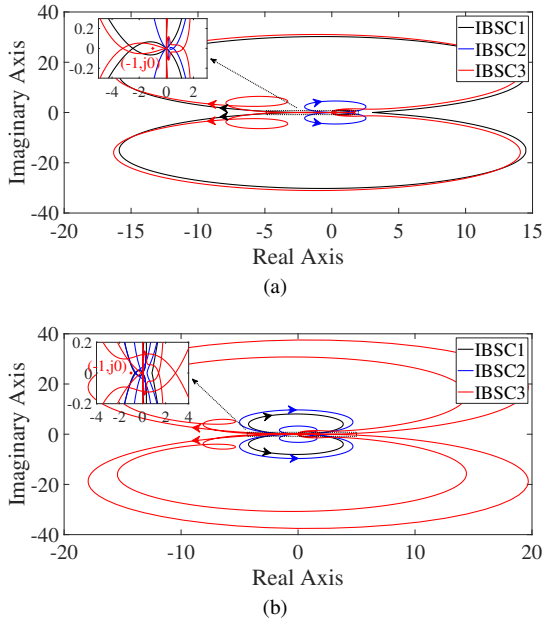

Fig. 8. Nyquist plots of three impedance ratios of case 1. (a) Scenario 1; (b) Scenario 2.

Nyquist plots are drawn in Fig. 8(b) again. It can be seen that all of them do not encircle point (-1, j0), which indicates that the system is globally stable.

B. Case 2: Modified CIGRE Low Voltage Distribution System

CIGRE low voltage distribution system as shown in Fig. 9 is used to validate the proposed impedance-decoupled network modelling method [27], where three scenarios are investigated.

1) Scenario 1: Parameters of the eight GCIs are assumed as the same and shown in the third column of Table I. Parameters of TLs are referred from [27] and modified in Table II. R4, R6 and R9 are modified as three, four and five TLs-based nodes as defined in Fig. 1. The impedance-decoupled network model can be established in Fig. 10, where voltage-controlled current sources are omitted for simplicity. It can be seen that nodes R4, R6 and R9-related TLs are modelled as three, four and five-ports impedance models, respectively, as shown in the red dotted boxes in Fig. 10. Then, Z_{15sh}/Z_{inv8}, Z_{24sh}/Z'_{12sh}, Z_{31sh}/Z'_{22sh} and Z_g/Z'_{32sh} can be calculated sequentially to assess system stability at different points. Instability point can be located once any impedance ratio does not satisfy Nyquist stability criterion.

Based on the parameters in Table I and Table II, impedance formulas of the impedance-decoupled network model of transmission network can be calculated using (6), (9) and (11). Nyquist plots of the four impedance ratios are drawn in Fig. 11. It can be seen that the Nyquist plot IBSC3 encircles point (-1, j0) one time, which indicates that the system is unstable.

2) Scenario 2: To verify that the proposed impedance-decoupled network modelling method is applicable when transmission network topologies or parameters change, stability issue of scenario 2 is investigated, where GCI 2 is connected to node R6 via a TL in the same electrical parameters as TL R6-R16. In addition, resistance of TL R10-R18 is 34.56 mΩ, and inductance of TL R10-R18 is 43.7358μH. Due to the modular impedance modelling characteristics, the established impedance models of GCI units and transmission networks are re-connected according to the new network topology. Nyquist plots of the four impedance ratios are drawn in Fig. 12(a). It can be seen that all Nyquist plots do not encircle point (-1, j0), which indicates that the power plant is globally stable.

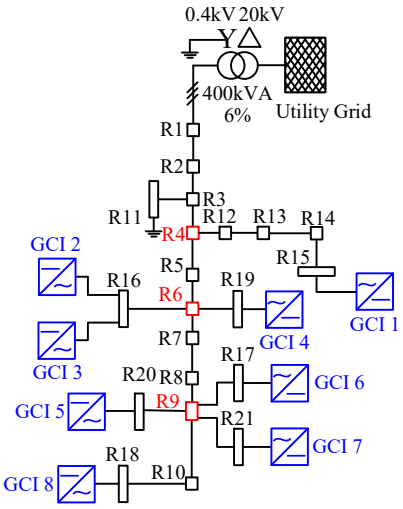

Fig. 9. Modified CIGRE low voltage distribution system [27].

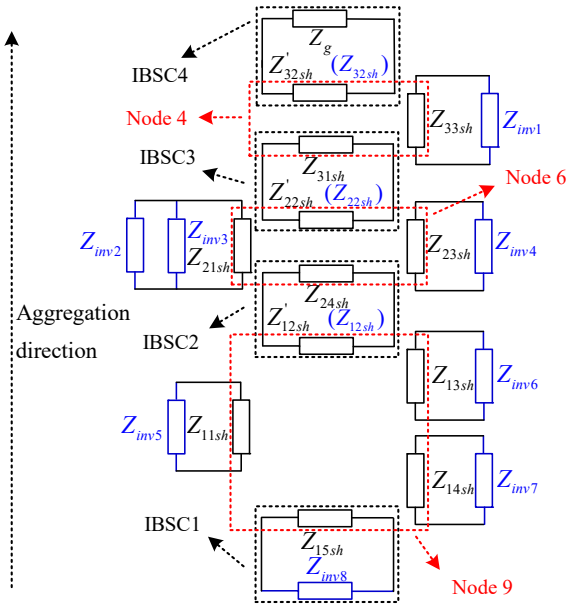

Fig. 10. Impedance-decoupled network model of the power plant in Fig. 9.

3) Scenario 3: Resistance of TL R6-R9 is 100.45mΩ, and inductance of TL R6-R9 is 186.0520μH. Nyquist plots of the four impedance ratios are drawn in Fig. 12(b) again. It can be seen that Nyquist plot IBSC2 encircles point (-1, j0) one time, which indicates that the system is unstable. It can be concluded that the impedance interaction at node R9 results in the instability phenomenon.

TABLE II
ELECTRICAL PARAMETERS OF TLS IN FIG. 9.

Node (From-To)	Resistance [mΩ]	Inductance [μH]
R1-R2	10.045	18.6052
R2-R3	10.045	18.6052
R3-R4	10.045	18.6052
R4-R6	20.09	37.2104
R6-R9	20.09	37.2104
R9-R10	10.045	18.6052
R4-R15	155.52	196.811
R6-R16	34.56	43.7358
R9-R17	34.56	43.7358
R10-R18	172.80	218.68
R6-R19	20.09	37.2104
R9-R20	15.0675	27.9078
R9-R21	15.0675	27.9078
Transformer	3.2	40.7437

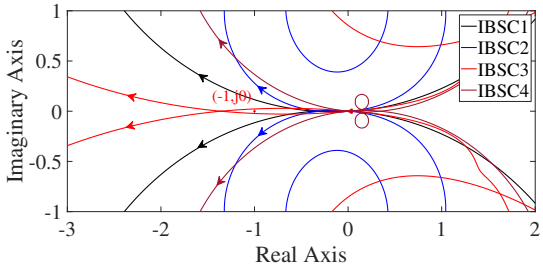

Fig. 11. Nyquist plots of four impedance ratios of scenario 1 of case 2.

V. SIMULATION AND EXPERIMENTAL VERIFICATION

In this section, time-domain simulations in Matlab/Simulink and experiments are implemented to validate effectiveness of the proposed impedance-decoupled network modelling and stability analysis method. Fig. 13 shows configuration of the experimental setup, which is composed of three Danfoss frequency converters (5kW), DC power source (750V), isolated

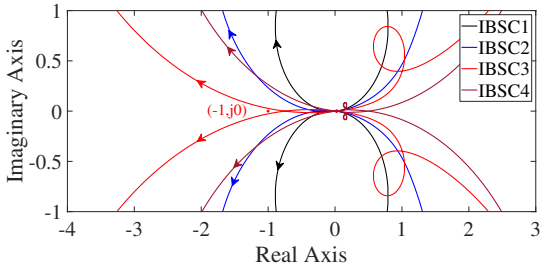

(a)

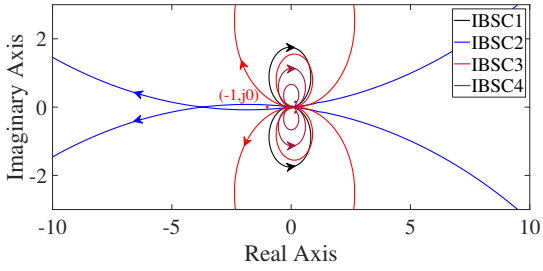

(b)

Fig. 12. Nyquist plots of four impedance ratios of case 2 by connecting GCI 2 to node R6. (a) Scenario 2; (b) Scenario 3.

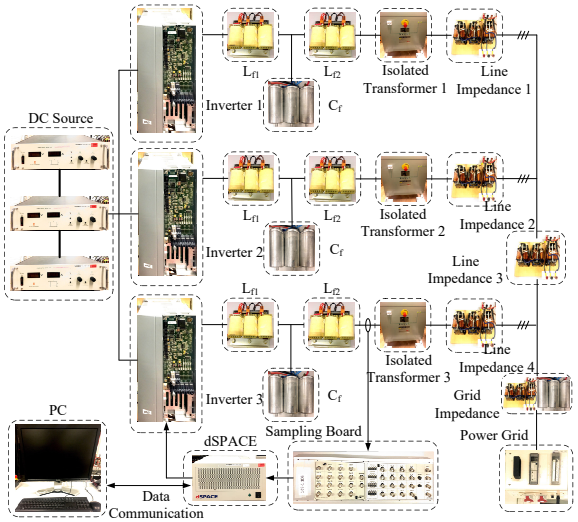

Fig. 13. Configuration of experimental setup.

transformers and LCL filters. Inductors and capacitors are used to emulate the TLs and grid impedance. The whole platform is controlled by dSPACE 1006 with a sampling period of 100 μs.

A. Case 1: Three GCIs-based Radial Power Plant

The parameters of the three GCIs are shown in the second column of Table I. If $L_{TL1} = L_{TL5} = L_{TL6} = 5$mH, $L_{TL2} = L_{TL3} = L_{TL4} = 0.5$mH, $C_g = 14\mu$F, $L_g = 1$mH and $R_g = 0.1\Omega$, Fig. 14(a) shows time-domain simulation result about unstable grid current i_g of scenario 1, and Fig. 14(b) shows time-domain simulation result about stable grid current i_g of scenario 2, where L_{TL1} is decreased from 5mH to 1mH. It can be seen that time-domain simulation results in Fig. 14 agree with stability analysis result in Fig. 8 for both unstable and stable cases. The impedance-decoupled network model-based multi-step IBSC can predict the instability phenomenon of radial power plant. Furthermore, experimental results shown in Fig. 15 are given to validate effectiveness of the proposed impedance-decoupled network modelling method. It can be seen that experimental results in Fig. 15 agree with both theoretical analysis results as shown in Fig. 8 and time-domain simulation results as shown in Fig. 14.

B. Case 2: Modified CIGRE Low Voltage Distribution Test System

Simulation verification is implemented in a modified CIGRE low voltage test system as shown in Fig. 9, where the system parameters are given in Table I and Table II. Fig. 16 shows simulation result about grid current i_g of scenario 1. It can be seen that time-domain simulation result in Fig. 16 agrees with the stability analysis result in Fig. 11. In addition, GCI 2 is connected to node R4 via a TL in the same electrical parameters as TL R6-R16. The parameters of TL R10-R18 are changed from 172.80mΩ, 218.68μH to 34.56 mΩ, 43.7358μH. Fig. 17(a) shows simulation result about grid current i_g of scenario 2. Furthermore, length of

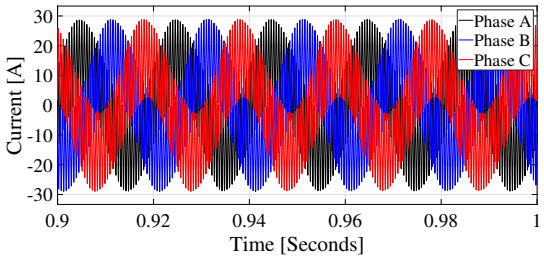

(a)

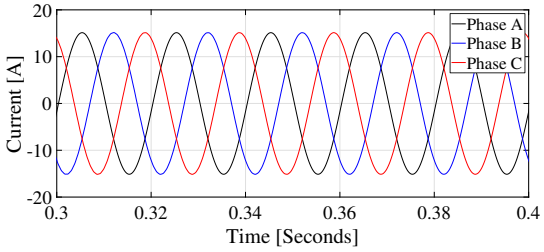

(b)

Fig. 14. Time-domain simulation results of grid current i_g of case 1. (a) Scenario 1; (b) Scenario 2.

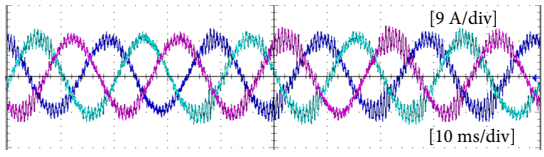

(a)

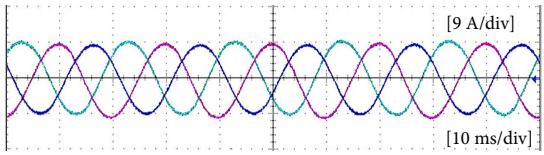

(b)

Fig. 15. Experimental results of grid current i_g of case 1. (a) Scenario 1; (b) Scenario 2.

TL R6-R9 increases with resistance increasing from 20.09mΩ to 100.45mΩ and inductance increasing from 37.2104μH to 186.0520μH, time-domain simulation result of grid current i_g of scenario 3 is shown in Fig. 17(b). It can be seen that time-domain simulation results as shown in Fig. 17 agree with stability analysis result as shown in Fig. 12 for both stable and unstable cases, which shows that the impedance-decoupled network model-based multi-step IBSC can predict instability phenomena in the low voltage test system. In addition, the proposed impedance-decoupled network modelling method is applicable in GCI-based power plant with various transmission network.

VI. Conclusion

This paper presents a decoupled multi-port impedance modelling method of inverter-fed power plant with complicated transmission network. Multi-port impedance model of transmission network is established by means of Norton equivalent circuit. Furthermore, stability analysis based on proposed

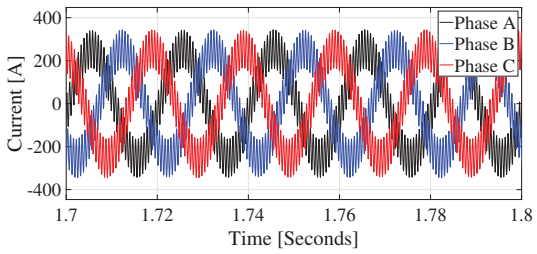

Fig. 16. Time-domain simulation result of grid current i_g of scenario 1 of case 2.

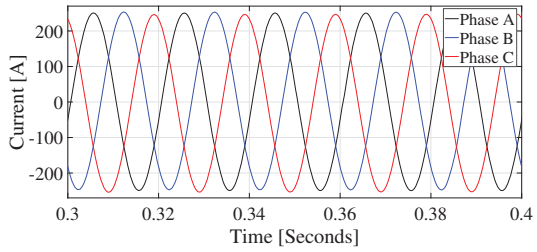

(a)

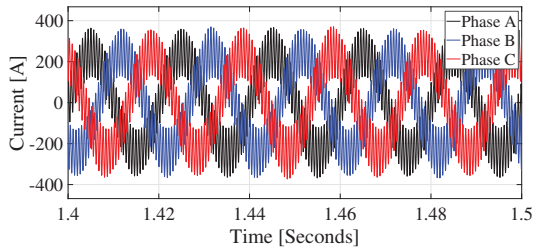

(b)

Fig. 17. Time-domain simulation results of grid current i_g of case 2 by connecting GCI 2 to node R6. (a) Scenario 2; (b) Scenario 3.

impedance network modelling method is performed. Simulation and experimental results are given to valid effectiveness of the proposed decoupled impedance network modelling method and stability analysis procedure. The stability analysis shows that the proposed decoupled multi-port impedance modelling method is able to simplify modelling procedure of transmission network, which can easily perform stability assessment in inverter-fed power plant with complicated transmission network. Also, the modelling method can identify oscillation source, and can be flexibly applied in various multiple branch-based transmission network.

References

[1] F. Blaabjerg, Z. Chen, and S. B. Kjaer, "Power electronics as efficient interface in dispersed power generation systems," *IEEE Trans. Power Electron.*, vol. 19, no. 5, pp. 1184–1194, Sep. 2004.

[2] J. H. Enslin and P. J. Heskes, "Harmonic interaction between a large number of distributed power inverters and the distribution network," *IEEE Trans. Power Electron.*, vol. 19, no. 6, pp. 1586–1593, Nov. 2004.

[3] Y. Wang, X. Wang, Z. Chen, and F. Blaabjerg, "Small-signal stability analysis of inverter-fed power systems using component connection method," *IEEE Trans. Smart Grid*, vol. 9, no. 5, pp. 5301–5310, Sep. 2018.

[4] H. Liu, X. Xie, J. He, T. Xu, Z. Yu, C. Wang, and C. Zhang, "Subsynchronous interaction between direct-drive PMSG based wind farms and weak AC networks," *IEEE Trans. Power Syst.*, vol. 32, no. 6, pp. 4708–4720, Nov. 2017.

[5] Y. Wang, X. Wang, F. Blaabjerg, and Z. Chen, "Harmonic instability assessment using state-space modeling and participation analysis in inverter-fed power systems," *IEEE Trans. Ind. Electron.*, vol. 64, no. 1, pp. 806–816, Jan. 2017.

[6] X. Wang and F. Blaabjerg, "Harmonic stability in power electronic-based power systems: Concept, modeling, and analysis," *IEEE Trans. Smart Grid*, vol. 10, no. 3, pp. 2858–2870, May 2019.

[7] J. Sun, "Impedance-based stability criterion for grid-connected inverters," *IEEE Trans. Power Electron.*, vol. 26, no. 11, pp. 3075–3078, Nov. 2011.

[8] W. Zhou, Y. Wang, and Z. Chen, "Decoupled multi-port impedance modelling method of transmission network in inverter-fed power plant," in *Proc. 2018 IEEE International Conference on Smart Grid (icSmartGrid)*, pp. 129–135.

[9] C. Yoon, H. Bai, X. Wang, C. L. Bak, and F. Blaabjerg, "Regional modeling approach for analyzing harmonic stability in radial power electronics based power system," in *Proc. 2015 IEEE Power Electronics for Distributed Generation Systems (PEDG)*, pp. 1–5.

[10] W. Cao, X. Zhang, Y. Ma, and F. Wang, "Stability criterion and controller parameter design of radial-line renewable systems with multiple inverters," in *Proc. 2016 IEEE Applied Power Electronics Conference and Exposition (APEC)*, pp. 2229–2236.

[11] W. Cao, Y. Ma, and F. Wang, "Sequence-impedance-based harmonic stability analysis and controller parameter design of three-phase inverter-based multibus AC power systems," *IEEE Trans. Power Electron.*, vol. 32, no. 10, pp. 7674–7693, Oct. 2017.

[12] J. L. Agorreta, M. Borrega, J. Lopez, and L. Marroyo, "Modeling and control of N-paralleled grid-connected inverters with LCL filter coupled due to grid impedance in PV plants," *IEEE Trans. Power Electron.*, vol. 26, no. 3, pp. 770–785, Mar. 2011.

[13] J. He, Y. W. Li, D. Bosnjak, and B. Harris, "Investigation and active damping of multiple resonances in a parallel-inverter-based microgrid," *IEEE Trans. Power Electron.*, vol. 28, no. 1, pp. 234–246, Jan. 2013.

[14] M. Lu, X. Wang, P. C. Loh, and F. Blaabjerg, "Resonance interaction of multiparallel grid-connected inverters with LCL filter," *IEEE Trans. Power Electron.*, vol. 32, no. 2, pp. 894–899, Feb. 2017.

[15] Y. Wang, X. Wang, F. Blaabjerg, and Z. Chen, "Frequency scanning-based stability analysis method for grid-connected inverter system," in *Proc. 2017 IEEE Future Energy Electronics Conference and ECCE Asia (IFEEC-ECCE Asia)*, pp. 1575–1580.

[16] W. Zhou, Y. Wang, D. Liu, and Z. Chen, "Optimization of active and reactive power dispatch among multi-paralleled grid-connected inverters considering low-frequency stability," in *Proc. IEEE 2019 45th Annual Conference of the IEEE Industrial Electronics Society (IES)*, pp. 6024–6031.

[17] Q. Ye, R. Mo, Y. Shi, and H. Li, "A unified impedance-based stability criterion (UIBSC) for paralleled grid-tied inverters using global minor loop gain (GMLG)," in *Proc. 2015 IEEE Energy Conversion Congress and Exposition (ECCE)*, pp. 5816–5821.

[18] C. Yoon, H. Bai, R. N. Beres, X. Wang, C. L. Bak, and F. Blaabjerg, "Harmonic stability assessment for multiparalleled, grid-connected inverters," *IEEE Trans. Sustain. Energy*, vol. 7, no. 4, pp. 1388–1397, Oct. 2016.

[19] Y. Wang, X. Wang, F. Blaabjerg, and Z. Chen, "Harmonic resonance assessment of multiple paralleled grid-connected inverters system," in *Proc. 2017 IEEE Future Energy Electronics Conference and ECCE Asia (IFEEC-ECCE Asia)*, pp. 2070–2075.

[20] X. Zhang, H. S.-h. Chung, L. L. Cao, J. P. W. Chow, and W. Wu, "Impedance-based stability criterion for multiple offshore inverters connected in parallel with long cables," in *Proc. 2017 IEEE Energy Conversion Congress and Exposition (ECCE)*, pp. 3383–3389.

[21] C. Wan, M. Huang, K. T. Chi, and X. Ruan, "Effects of interaction of power converters coupled via power grid: A design-oriented study," *IEEE Trans. Power Electron.*, vol. 30, no. 7, pp. 3589–3600, Jul. 2015.

[22] M. Amin and M. Molinas, "A gray-box method for stability and controller parameter estimation in HVDC-connected wind farms based on nonparametric impedance," *IEEE Trans. Ind. Electron.*, vol. 66, no. 3, pp. 1872–1882, Mar. 2019.

[23] H. Liu, X. Xie, and W. Liu, "An oscillatory stability criterion based on the unified *dq*-frame impedance network model for power systems with high-penetration renewables," *IEEE Trans. Power Syst.*, vol. 33, no. 3, pp. 3472–3485, May 2018.

[24] H. Liu and X. Xie, "Impedance network modeling and quantitative stability analysis of sub-/super-synchronous oscillations for large-scale wind power systems," *IEEE Access*, vol. 6, pp. 34 431–34 438, 2018.

[25] W. Zhou, Y. Wang, and Z. Chen, "Impedance-based modelling method for length-scalable long transmission cable for stability analysis of grid-connected inverter," in *Proc. 2018 IEEE 4th Southern Power Electronics Conference (SPEC)*, pp. 1–8.

[26] M. Cheah-Mane, L. Sainz, J. Liang, N. Jenkins, and C. E. Ugalde-Loo, "Criterion for the electrical resonance stability of offshore wind power plants connected through HVDC links," *IEEE Trans. Power Syst.*, vol. 32, no. 6, pp. 4579–4589, Nov. 2017.

[27] K. Strunz, N. Hatziargyriou, and C. Andrieu, "Benchmark systems for network integration of renewable and distributed energy resources," Cigre Task Force C6: 04-02, 2014.